Increasing the coupling efficiency in a heavy ion, inertial confinement fusion target

D.A. Callahan-Miller, M. Tabak

Lawrence Livermore National Laboratory,
Livermore, California,
United States of America

Abstract. A close coupled, distributed radiator heavy ion target is presented. Close coupled refers to a decrease in the distance between the hohlraum wall and the inertial confinement fusion capsule. In two dimensional, integrated, LASNEX calculations, this target produced 436 MJ of yield from 3.27 MJ of ion beam energy for a gain of 133. To achieve these results, the hohlraum dimensions were reduced by 27% from the previous distributed radiator, heavy ion target while driving the same capsule. This reduced the beam energy required from 5.9 to 3.27 MJ. Calculations of single mode Rayleigh–Taylor growth for this capsule show that this capsule is more stable than at least one of the NIF target designs (the PT design which uses a CH ablator doped with oxygen and bromine). This means that issues regarding the Rayleigh–Taylor instability for the heavy ion driven capsule can be settled on NIF. This close coupled target can also be scaled down in size for an Engineering Test Facility; LASNEX calculations predict that a gain of 94 can be achieved from 1.75 MJ of beam energy. In addition, gain curves for distributed radiator targets with the 'conventional' case to capsule ratio and the close coupled case to capsule ratio are presented.

1. Introduction

There is a spectrum of possible inertial confinement fusion targets. At one end is a direct drive target in which the beam (ion or laser) energy is directly deposited on the capsule [1, 2]. Direct drive is the most efficient method of imploding a capsule because a large fraction of the beam energy is coupled to the capsule. At the other end of the spectrum is an indirect drive target in which the beam energy is converted to X rays in a hohlraum. The X rays then transport the energy to the capsule. Indirect drive is less efficient because much of the beam energy goes into heating the hohlraum walls. While less efficient than direct drive, indirect drive has advantages in uniformity since the radiation transport smooths out the high frequency oscillations. In addition, radiation drive has higher hydrodynamic efficiency and improved stability properties compared with direct drive.

Heavy ion driven inertial confinement fusion has generally favoured indirect drive targets. Because accelerators are efficient (∼25–35%), gains as low as 30–40 still produce an efficiency gain product (ηG) greater than the 8–10 needed for a power plant. The low gain requirement means that a high coupling efficiency is not necessary, and the irradiation uniformity advantages of indirect drive targets are attractive. In addition, indirect drive targets are better suited to two sided illumination, which has advantages for power plant design [3].

On the other hand, the cost of the accelerator increases as the beam energy required increases. One method for reducing the cost of the accelerator is to reduce the necessary beam energy by increasing the coupling efficiency from the beams to the capsule. To accomplish this, we have reduced the size of the hohlraum surrounding the capsule. By doing so, we reduce the amount of energy going into the hohlraum wall and increase the coupling. By starting with an indirect drive target and moving towards a more closely coupled, indirect drive target, many of the advantages of indirect drive are retained.

In this article, we present LASNEX [4] calculations of a close coupled target that produced a yield of 436 MJ from 3.27 MJ of ion beam energy. In addition to describing the target, we show results from single mode, Rayleigh–Taylor calculations of this capsule. In these Rayleigh–Taylor calculations, we include the radiation converter because its proximity to the capsule could have an impact on the ablative stabilization of the Rayleigh–Taylor instability. Finally, we present gain curves for these types of targets.

2. Close coupled target design

Our goal for the close coupled, distributed radiator target was to reduce the beam energy required from 5.9 MJ [5–7] to 3.5 MJ by reducing the hohlraum size while driving the same capsule. We

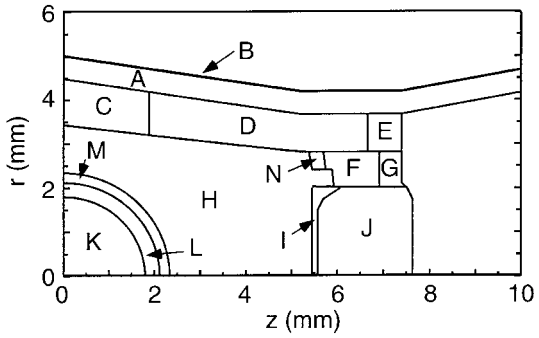

Figure 1. Diagram of a quarter of the capsule and hohlraum for the close coupled target. The complete target can be formed from a rotation about the z axis and a reflection about the r axis. The materials and densities used were as follows: A, AuGd at 0.1 g/cm^3; B, 15 μm layer of AuGd at 13.5 g/cm^3; C, Fe at 16 mg/cm^3; D, $(CD_2)_{0.97}Au_{0.03}$ at 11 mg/cm^3; E, AuGd at 0.11 g/cm^3; F, Al at 70 mg/cm^3; G, AuGd at 0.26 g/cm^3; H, CD_2 at 1 mg/cm^3; I, Al at 55 mg/cm^3; J, AuGd sandwich with densities 0.1 g/cm^3, 1.0 g/cm^3 and 0.5 g/cm^3; K, DT at 0.3 mg/cm^3; L, DT at 0.25 g/cm^3; M, $Be_{0.995}Br_{0.005}$ at 1.845 g/cm^3; N, $(CD_2)_{0.97}Au_{0.03}$ at 32 mg/cm^3.

began with a distributed radiator target [5–7] that had a 'conventional' case to capsule ratio. In the distributed radiator target, most of the hohlraum is filled with converter material that converts the beam energy into X rays which then drive the capsule. As a shorthand, we refer to the distributed radiator target that has a conventional case to capsule ratio as the 'conventional distributed radiator target' and the distributed radiator target that has a close coupled case to capsule ratio as the 'close coupled target'. In the conventional distributed radiator target, the energy distribution was as follows: 1.09 MJ in the converters (although the dimensions in Fig. 1 are for the close coupled target, regions C, D, E, F, G and N represent this part of the target for both the close coupled and conventional distributed radiator targets), 2.84 MJ in the wall (regions A and B in Fig. 1), 0.25 MJ in the beam block (regions I and J in Fig. 1), 0.67 MJ escaped (energy radiated away mainly from the outer surface of regions E and G in Fig. 1) and 1.02 MJ in the capsule (regions K, L and M in Fig. 1). In the close coupled target, most of the hohlraum dimensions were scaled by a factor of 0.736. The energy into the converters E_{con} scales as the volume, while the energy into the wall E_{wall} and beam block E_{bl}, as well as the escaped energy E_{esc}, scale as the area. The energy into the capsule E_{cap} is unaffected. A target scaled by 0.736 should then use

$$\begin{aligned} E_{beam} &= l^3 E_{con} + l^2(E_{wall} + E_{bl} + E_{esc}) + E_{cap} \\ &= (0.736)^3(1.09) + (0.736)^2(2.84 + 0.25 + 0.67) \\ &\quad + 1.02 \\ &= 3.5 \text{ MJ}. \end{aligned} \tag{1}$$

In the close coupled design, about 28% (1 out of 3.5 MJ) of the beam energy is coupled to the capsule. For comparison, the earlier heavy ion target has about 17% (1 out of 5.9 MJ) of the beam energy absorbed by the capsule. The NIF target has about 11–15% (0.15–0.2 out of 1.35 MJ) of the laser energy absorbed by the capsule [8, 9]. Of course, the NIF baseline target must be conservative; efforts are already under way to design NIF targets with higher coupling efficiency [10]. Target features such as low density walls designed to be in pressure balance with the hohlraum fill, which are used in the close coupled target presented here, allow us to move the hohlraum wall closer to the capsule. These features may also be used in future laser targets.

2.1. Scaling the target

The hohlraum and capsule used in the close coupled design are shown in Figs 1 and 2 with capsule dimensions $r_{abl} = 2.34$ mm, $r_{fuel} = 2.12$ mm and $r_{gas} = 1.8$ mm. The hohlraum is mainly a scaling of conventional distributed radiator design [7]; the major differences between a simple scaling and the hohlraum shown in Fig. 1 are:

(a) A larger beam block radius to hohlraum radius ratio,
(b) A larger 'tilt' to the hohlraum wall over the capsule waist,
(c) A 10% larger ratio of hohlraum length to radius.

The size of the beam block is determined by the size of the capsule and so it is not scaled. This means that the radius of the ion beams is reduced by more than 0.736. For this design, we assumed the same number of beams as we did for the conventional distributed radiator target (8 beams per side in the low power, foot pulse and 16 beams per side in the main pulse) and the same beam geometry (elliptical beams overlayed to form an annulus on the end of the hohlraum) [7]. The beams used in this calculation were elliptically shaped with major and minor axes of 2.78 and 1.0 mm for an 'effective' radius $\sqrt{ab} = 1.67$ mm. The beams were assumed to have a

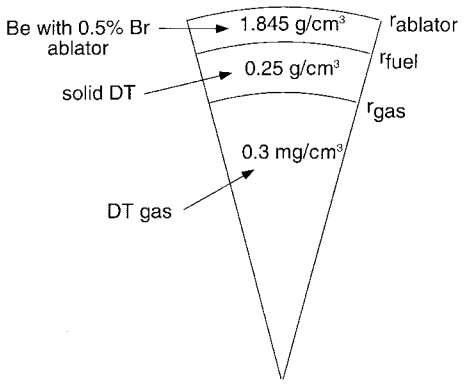

Figure 2. Pie diagram of the capsule. The capsule uses cryogenic DT fuel and a beryllium ablator doped with 0.5% bromine.

Gaussian distribution and this ellipse is the one that contains 95% of the charge.

It should be noted that in this geometry all the beams cross just upstream of the target. The deflections that result from this crossing may make it more difficult to achieve the small beam spots that this target requires. Experiments and detailed simulations of the ion beams in the accelerator and reactor chamber will be needed to determine whether beam spots of this size can be achieved.

Because the beam block size was kept constant, the beam centroids were aimed closer to the hohlraum wall. In particular, the beam centroids hit the end of the hohlraum at a radius of 2.8 mm roughly where regions E and G intersect in Fig. 1. To accommodate the beam entrance angles (6° in the foot and 12° in the main pulse), the radius of the hohlraum at the capsule waist was increased. If the radius of the hohlraum near the capsule waist was not increased, too much of the beam energy was deposited in the hohlraum wall causing symmetry problems.

2.2. Symmetry issues

To analyse the time dependent asymmetry of the target, we monitor the time integrated pressure ($\int_0^t P(t')dt'$) near the ablation front as a function of time. We then decompose this pressure into Legendre moments, P_2, P_4, etc. and compare these values with P_0. Because the orthogonality condition for the Legendre polynomials is

$$\int_{-1}^{1} P_{l'}(x)P_l(x)dx = \frac{2}{(2l+1)}\delta_{l,l'} \qquad (2)$$

we need to multiply the decomposed values by $2l + 1$ before comparing them with the P_0 component. For example, if the pressure is written as $Pr(x) = \sum \alpha_l P_l(x)$, then

$$(2l+1)\int_{-1}^{1} P_l(x)Pr(x)dx = 2\alpha_l. \qquad (3)$$

The odd moments, P_1, P_3, etc. are assumed to be zero due to left–right symmetry.

Our initial calculations of the close coupled target used the same hohlraum length to radius ratio as the conventional distributed radiator target and had problems with P_4 asymmetry. Radiation uniformity is a big issue in the close coupled target, because the smaller case to capsule ratio results in less radiation smoothing due to transport. P_4 asymmetries can be tuned out by adjusting the ratio of the hohlraum length to radius because this changes the location of the sources relative to the zeros of P_4. In distributed radiator targets, the sources of radiation are placed near the zeros of P_4 and weighted such that P_2 is approximately cancelled. Figure 3 shows the P_4 component of the time integrated pressure (scaled up 9×) measured near the ablation front as a function of time for two calculations. The lower curve shows the

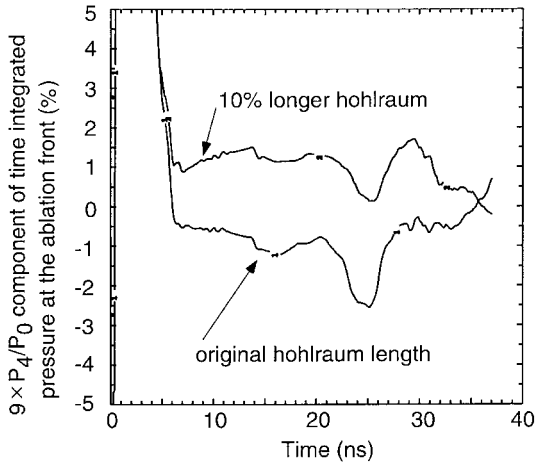

Figure 3. The $9 \times P_4$ component of the time integrated pressure ($\int_0^t P(t')dt'$) measured near the ablation front as a function of time for two calculations. The factor of 9 is included because of the normalization for the Legendre polynomials. The lower curve shows the original hohlraum length while the upper curve shows a 10% longer hohlraum. In the distributed radiator targets, the energy is deposited near the zeros of the fourth Legendre polynomial P_4 and weighted such that P_2 is small. The P_4 asymmetry is tuned by changing the ratio of hohlraum length to hohlraum radius. A 10% change in hohlraum length (at fixed radius) results in a 2% change in the P_4 asymmetry at the capsule.

original hohlraum length to radius and the upper curve shows a 10% increase in the hohlraum length (with fixed radius). The 10% longer hohlraum shows a smaller swing in asymmetry, about 1.5% around 30 ns, than the original hohlraum length, which had a maximum asymmetry swing of about 2.5% around 25 ns. Although one calculation with the original hohlraum length did ignite, the radiation uniformity was very marginal. Increasing the hohlraum length by 10% caused a 6% increase in beam energy but produced a more robust implosion. Figure 3 may indicate increasing the hohlraum length by 5% instead of 10% would produce even better symmetry and with a smaller energy penalty.

Because the radiation smoothing is reduced in the close coupled target, we were careful to adequately resolve the P_6 and P_8 modes in the calculation. Thirty-two angular zones were used around the 90° quadrant of the capsule shown in Fig. 1. The zoning in the hohlraum was essentially the same as that used in calculations of the conventional distributed radiator target, which is shown in Fig. 1 of Ref. [5] or Fig. 6 of Ref. [6]. The time dependent asymmetry is shown in Fig. 4. As in the conventional distributed radiator target, the ion kinetic energy was changed to overcome range shortening. In this case, the ion energy was increased from 2.2 to 3.5 GeV at 24 ns; the change in ion energy is seen in the asymmetry as the P_2 component changes slope around 24 ns.

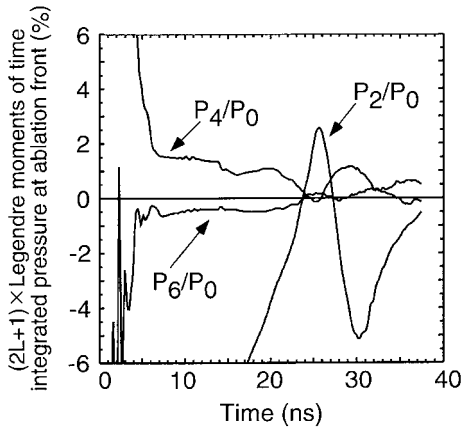

Figure 4. Time dependent asymmetry is monitored by measuring the time integrated pressure at the ablation front and decomposing into Legendre moments. The change in slope of the P_2 moment at 24 ns is due to the change in ion kinetic energy between the foot and main pulse beams.

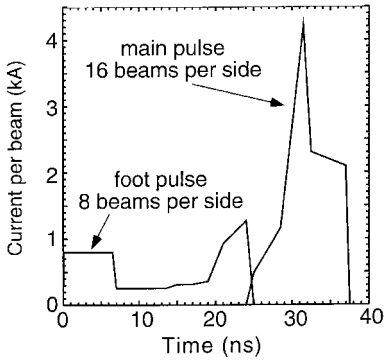

Figure 5. Beam current as a function of time used in the 2-D integrated LASNEX calculations assuming a total of 16 beams in the foot (8 per side) and 32 beams in the main pulse (16 per side).

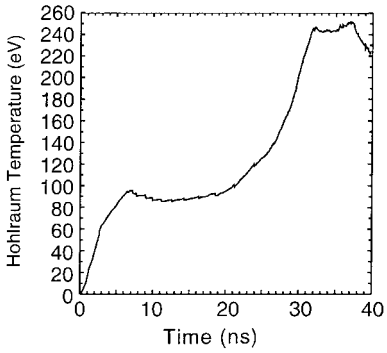

Figure 6. Hohlraum temperature as a function of time from the 2-D integrated calculation of the close coupled target.

2.3. Target performance

The target shown in Fig. 1 produced 436 MJ of yield from 3.27 MJ of ion beam energy in 2-D integrated LASNEX calculations. This represents a gain of 133. Figure 5 shows the beam current used to drive the target as a function of time. In the foot, 0.49 MJ of 2.2 GeV Pb^+ ions were used, while the main pulse was made up of 2.78 MJ of 3.5 GeV Pb^+ ions. This corresponds to a peak power of 470 TW. Our conventional distributed radiator design (5.9 MJ target) had a peak power of 650 TW; the peak power in the close coupled target did not drop as much as would be expected from the energy decrease because of the pulse shape used. Future calculations will explore pulse shapes that result in lower peak power and that are easier for the accelerator to produce.

The hohlraum temperature driving the capsule is shown in Fig. 6. The peak temperature is about 10 eV lower than the temperature used to drive our previous calculations. This decrease in drive

temperature accounts for the fact that less than 3.5 MJ of beam energy (as the scaling would predict) was needed even though the hohlraum length was increased by 10%.

3. Rayleigh–Taylor instability for the close coupled target

Single mode, linear, Rayleigh–Taylor calculations, similar to those done for the NIF targets, show growth factors that are the same or smaller than those calculated for NIF. In these calculations, a small perturbation was introduced on the surface of the ablator. The calculation was then driven by a temperature source placed in the low density gas region surrounding the capsule (Fig. 7). The linear growth factor was measured by finding the size of the perturbation that had fed through to the outside of the hot spot at ignition time divided by the size of the initial perturbation. We ran these calculations for a variety of modes ranging from $l = 30$ (12° per wavelength) to $l = 240$ (1.5° per wavelength) and found that all the growth factors were less than 300 (see Fig. 8).

As is shown in Fig. 7, we tried to include the effect of the converter over the waist of the capsule. Since this converter is located very close to the capsule in the close coupled design, we were concerned that it could affect the ablative stabilization and increase

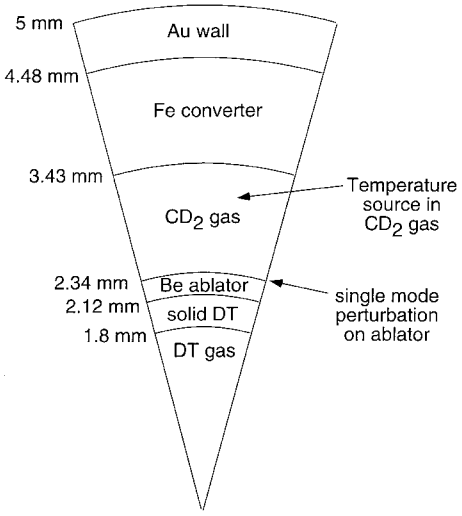

Figure 7. Pie diagram of the simulation region for the 2-D Rayleigh–Taylor instability calculations. The iron converter over the capsule waist is included in the calculations to determine its effect on the Rayleigh–Taylor growth rates.

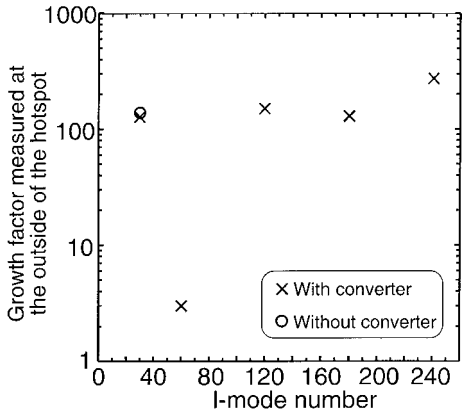

Figure 8. Linear, single mode, Rayleigh–Taylor growth factors as a function of mode number. One calculation at mode 30 (denoted by the circle) was done without the iron converter over the capsule waist for comparison.

the growth rate for the Rayleigh–Taylor instability. In the Rayleigh–Taylor runs, the temperature source was placed in the gas because we wanted to be sure that we had an accurate source driving the capsule. In a real target, there is a source of radiation in the iron converter. This discrepancy in the location of the source could change the motion of the iron converter and change the converter's effect on the Rayleigh–Taylor instability. In Fig. 9, the solid curve shows the location of the gas–iron interface as a function of time for the Rayleigh–Taylor instability calculations. The crosses in Fig. 9 show the same interface from the 2-D integrated calculations. Since we do rezoning in the 2-D integrated calculations, the gas and ablator materials mix with the iron. The crosses show the point where 50% (by weight) of the material is iron. The error bars show the extent of the mixed layer; the lower end of the error bars is the point where 10% of the material is iron while the upper end of the error bars is the point where 90% of the material is iron. This figure indicates that even with the radiation source in the gas, the gas–iron interface is roughly correct.

To understand whether the iron converter was changing the Rayleigh–Taylor growth rate, we ran one calculation without the converter. The circle in Fig. 8 shows the growth factor for mode 30 without the converter and shows essentially the same growth as with the converter.

Lindl [11] found linear growth factors for one NIF design peaking around mode 30 with a maximum value of about 800. It is reassuring to see that our linear growth factors are smaller by a factor of two or more. This shows that our capsule is more

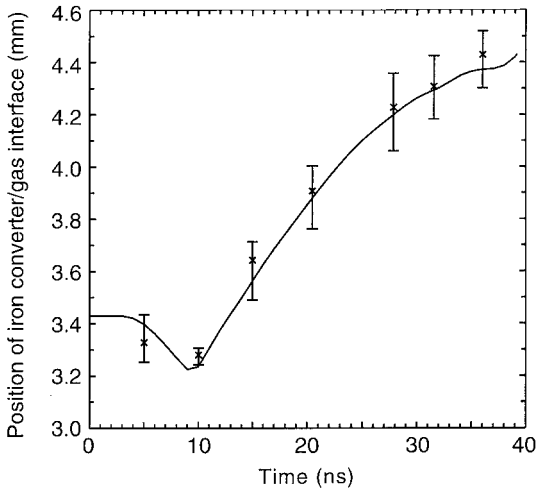

Figure 9. Location of the interface between the iron converter and the gas surrounding the capsule as a function of time. The solid curve shows the interface for the configuration used to model the Rayleigh–Taylor instability (which had the temperature source in the gas rather than in the converter). The crosses show the interface from the 2-D integrated calculation (which had a radiation source inside the converter). In the 2-D integrated calculations, rezoning causes the iron to mix with the gas and/or the ablator material. The crosses show the position where 50% (by weight) of the material is iron. The error bars indicate the width of the mixed layer by showing the positions where the material is 10% (lower end of the error bar) and 90% (upper end of the error bar) iron.

conservative than at least one NIF target; ignition on NIF will then demonstrate the stability of our capsule.

In addition, we can estimate how far perturbations due to the Rayleigh–Taylor instability will move into the hot spot assuming purely linear growth (i.e. no non-linear saturation) by multiplying (surface finish) × (growth factor) × (convergence ratio)/(initial ablator radius). For example, smooth NOVA capsules have a surface finish of about 300 Å [11, 12]. Using a growth factor of 300 (from Fig. 8) and a convergence ratio of 20–35 [11], we find that linear growth will cause perturbations to protrude 8–12% of the way into the hot spot. Again, this is more conservative than NIF, because not only is the growth factor smaller, but our hot spot radius (∼(initial ablator radius)/(convergence ratio)) is about a factor of two larger (since our initial ablator radius is a factor of two larger). This gives us confidence that issues about the Rayleigh–Taylor instability for the heavy ion capsule will be settled on NIF.

4. Close coupled target for an Engineering Test Facility

One of the goals of the inertial fusion energy program is to construct an Engineering Test Facility (ETF) that demonstrates all the physics and technology needed for an inertial fusion energy power plant. The ETF would be a high repetition rate, high gain facility, and would be used for testing chamber concepts, materials and advanced targets. Since the ETF would not be a power plant, it would not need the full yield required for 1 GW(e) operation. Provided the driver has adequate repetition rate, an ETF might be upgradable to a demonstration power plant by using multiple chambers with a beam switchyard, however.

To keep the cost of an ETF reasonable, a driver energy of 2 MJ or less will probably be required [13–15]. A scaled down version of the close coupled target could meet those requirements. One dimensional LASNEX calculations of a 0.77 scale version of our capsule (Fig. 2 with $r_{abl} = 1.80$ mm, $r_{fuel} = 1.63$ mm and $r_{gas} = 1.39$ mm) produced 183 MJ of yield when driven by the radiation temperature profile shown in Fig. 10.

We can make an estimate of the beam energy required to drive the ETF scale target by considering how each component of the target scales with length l, time τ and temperature T_r. The energy into the wall scales as [11]

$$E_{wall} \propto l^2 T_r^{3.3} \tau^{0.62}. \quad (4)$$

The energy into the capsule and beam block as well as the energy escaped scale as

$$E_{cap+bl+esc} \propto l^2 T_r^4 \tau. \quad (5)$$

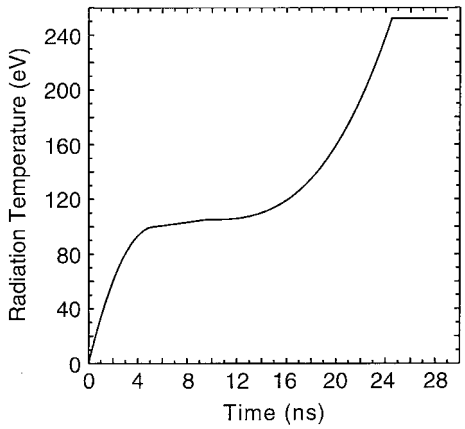

Figure 10. Temperature as a function of time used to drive the ETF scale capsule in 1-D. The capsule yield in 1-D was 183 MJ.

The energy into the converters scales as

$$E_{con} \propto l^3 T_r \tau. \tag{6}$$

In the 3.27 MJ close coupled target, the energy distribution was 1.52 MJ in the wall, 0.90 MJ in the capsule, 0.12 MJ in the beam block, 0.32 MJ escaped and 0.42 MJ in the converters. Scaling these energies to an ETF scale target assuming $l = 0.77, \tau = 0.77$ and $T_r = 252/240 = 1.05$ predicts 1.8 MJ of beam energy.

Two dimensional LASNEX calculations confirm these scalings. A 0.77 scale version of the close coupled target produced 165 MJ from 1.75 MJ of beam energy. The ion current per beam and resulting radiation temperature profiles are shown in Fig. 11. This represents a gain of 94.

The beam parameters must also be scaled with the target. The 0.77 scale target would require beams with an effective radius of 1.29 mm (0.77×2.1 mm). The ion range would also be decreased by 0.77; this decrease in range would correspond to a kinetic energy of about 3 GeV for Pb^+ ions. In addition, the pulse duration is also shorter by the same factor of 0.77. While the lower kinetic energy might make the accelerator less expensive, the smaller spot, shorter pulse duration and lower kinetic energy all make focusing the beam more difficult. These new requirements need to be evaluated in an integrated system including accelerator, final focus and chamber transport.

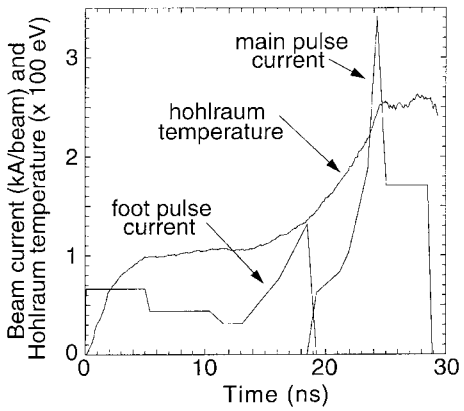

Figure 11. Ion current per beam as a function of time and the resulting hohlraum temperature from the 2-D integrated calculations of the ETF scale target. The beam currents assume 16 beams of 1.85 GeV Pb^+ ions in the foot pulse (8 per side) and 32 beams of 3 GeV Pb^+ ions in the main pulse (16 per side).

5. Gain curves for distributed radiator targets

It is useful to have gain curves for both the conventional and close coupled distributed radiator targets that can be used to rapidly study the tradeoffs between, for example, the target, accelerator and chamber in systems studies and power plant optimizations.

To calculate the gain curves, we begin by scaling to larger and smaller capsules following Lindl's Eqs (87) and (90) [11]. For a fixed in-flight aspect ratio ($R/\Delta R$), the amount of energy that the capsule must absorb is

$$E_{cap} \propto \beta^{-3/2} T_r^{-4.5} \tag{7}$$

where β is the adiabat (which we assume is constant) and T_r is the hohlraum temperature. For a given amount of energy absorbed by the capsule, we use this equation to calculate the hohlraum radiation temperature. The capsule radius then scales as

$$r_{cap} \propto \frac{\beta^{1/5} E_{cap}^{1/3}}{T_r^{1.03}} \tag{8}$$

and the pulse duration scales as

$$\tau \propto \frac{E_{cap}^{1/3}}{\beta^{2/5} T_r^{1.93}}. \tag{9}$$

Given the capsule size, the pulse duration and the hohlraum temperature, we then calculate the amount of beam energy needed to drive the hohlraum. We break the hohlraum up into several pieces: the wall (for the close coupled target, regions A and B in Fig. 1), the converters (regions C, D, E, F, G and N in Fig. 1) and the beam block (regions I and J in Fig. 1). To calculate the required beam energy, we need the energy in each of these pieces plus the capsule (regions K, L and M in Fig. 1) and the energy that escapes from the beam entrance 'window' (regions E and G in Fig. 1). The ratio of the hohlraum radius to the capsule radius is an input parameter and determines whether the gain curve is for a conventional distributed radiator target or a close coupled target.

The wall is heated by a Marshak wave and the energy into it is given by [11]

$$E_{wall} \propto r_{hohl}^2 T_r^{3.3} \tau^{0.62}. \tag{10}$$

As the hohlraum size is changed, the heat capacity of the converters can be scaled assuming either constant ion range (i.e. the converter density is changed

to make up for the change in hohlraum length) or variable ion range (i.e. the converter density is constant and the ion range changes as the hohlraum length changes). In the case of constant ion range, the energy into the converters varies as the hohlraum area,

$$E_{con} \propto r_{hohl}^2 T_r \tau \tag{11}$$

while the energy into the converters varies as the hohlraum volume in the case of variable ion range

$$E_{con} \propto r_{hohl}^3 T_r \tau. \tag{12}$$

The beam block (region J in Fig. 1) is heated by a Marshak wave from the inside of the hohlraum and by the beam on the outside of the hohlraum. With the beams overlaid to form an annulus, very little beam energy is deposited in the beam block so we assume that most of the energy absorbed by the block is from the Marshak wave,

$$E_{bl} \propto r_{cap}^2 T_r^{3.3} \tau^{0.62}. \tag{13}$$

To calculate the amount of energy that escapes through the annular beam entrance 'window' (regions E and G in Fig. 1), we follow the derivation of Ho et al. [16]. Since most of the energy loss occurs during the main pulse, when the beam power is roughly constant, it is assumed that the radiation flux from the surface S_0 has reached a steady state value. Since the window is optically thick, the radiation flux can be determined from a steady state diffusion equation. Ho et al. solved for the flux on the outside (side facing vacuum) of the window and found

$$S_0 \approx \frac{8\sigma}{9\alpha} \frac{T_r^{4+\beta}}{\delta} + \frac{q\delta}{2} \tag{14}$$

where σ is Boltzmann's constant, δ is the range (g/cm^2) of the window, T_r is the radiation temperature inside the hohlraum, q is the specific energy loss rate of the beam in the window (W/g), and α and β are constants used to fit the Rosseland mean free path. The Rosseland mean free path, l_R, is assumed to be of the form $l_R = \alpha T^\beta / \rho$. Comparing this form with that given by Lindl [11] for gold, we use $\beta = 1.5$ and $\alpha = 1/6000$ when T is measured in hundreds of electronvolts. The energy that escapes is then calculated using

$$E_{esc} \approx 2\pi (r_{hohl}^2 - r_{cap}^2) S_0 \tau. \tag{15}$$

The constants of proportionality used to find E_{wall}, E_{con} and E_{bl} were determined by using one of the 2-D integrated LASNEX calculations. For the gain curves shown below, the 6 MJ conventional distributed radiator target [7] was used. For that target, E_{cap} = 1.0 MJ, E_{wall} = (2.9 MJ)×1.1, E_{con} = 1.1 MJ, E_{bl} = 0.3 MJ and E_{esc} = 0.7 MJ when driven at 250 eV for 8 ns. The energy into the wall was increased by a factor of 1.1 to take into account the longer hohlraum used in the close coupled design (described in Section 2.2) to better tune out P_4. We suspect that our conventional distributed radiator target would also benefit from this change and so we included the extra energy in the gain curves.

To calculate the gain, we need the total driver energy and the yield. The driver energy is calculated by adding up all the components,

$$E_{dr} = E_{cap} + E_{wall} + E_{con} + E_{bl} + E_{esc}. \tag{16}$$

The yield is calculated by again using the scaling from Lindl,

$$Y \propto E_{cap}^{5/3}. \tag{17}$$

Finally, the gain is just the yield divided by the driver energy.

Gain curves for the conventional and close coupled distributed radiator targets are shown in Fig. 12. The three point designs (2-D integrated LASNEX calculations) are shown by the squares. In the integrated LASNEX calculations, the conventional distributed radiator target was driven at 250 eV, while the close coupled target was driven at 240 eV. The gain curves are plotted for both drive temperatures. The implications for the lower drive temperature on the ignition margin (defined as the fraction of the incoming kinetic energy of the fuel left at ignition) are currently under study, although preliminary calculations show that 240 eV is acceptable.

For the distributed radiator targets, the beam spot size is determined by the hohlraum radius and the capsule radius as is shown in Fig. 13. This means that for each target size, there is an associated beam spot size. Figures 14 and 15 show the beam spot sizes for the conventional distributed radiator target and the close coupled target, respectively, shown in the gain curves.

6. Conclusions

Two dimensional, integrated LASNEX calculations predict that a heavy ion target can produce a gain of 133 from 3.3 MJ of beam energy. In this close coupled target, 28% of the ion beam energy

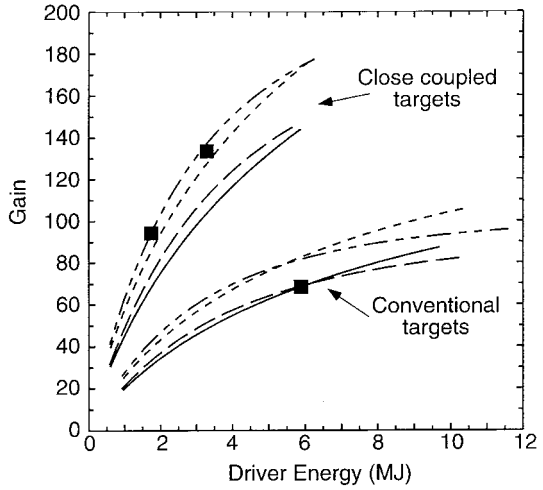

Figure 12. Gain curves for the distributed radiator targets. The lower set of curves is for the conventional case to capsule ratio, while the upper set is for the close coupled design. For each set, the solid curve is for 250 eV drive and fixed ion range (i.e. converter densities are increased (decreased) as hohlraum length is shortened (lengthened)), the dashed curve is for 250 eV drive and varying ion range (i.e. the ion range is shortened (lengthened) as the hohlraum length is shortened (lengthened)), the dotted curve is for 240 eV drive and fixed ion range and the chain curve is for 240 eV drive and varying ion range. The squares represent the three integrated LASNEX calculation point designs.

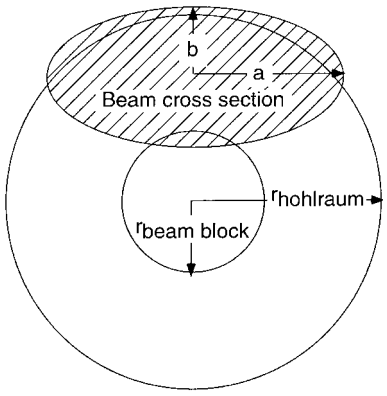

Figure 13. The dimensions of each beam are determined by the hohlraum radius and the beam block radius (which is related to the capsule radius). Each beam is assumed to have a Gaussian distribution and is focused to an elliptical spot. The semi-major and semi-minor axes shown in this figure are assumed to contain 95% of the beam. (The beams are chosen to slightly overfill the target.)

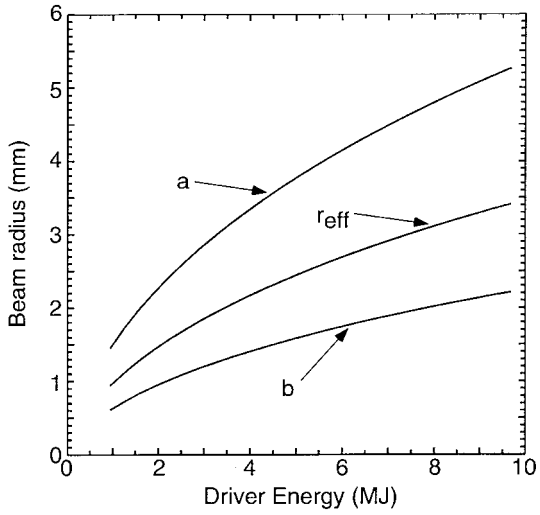

Figure 14. Beam spot sizes as a function of driver energy for the conventional case to capsule ratio. The curves are for 250 eV drive and fixed ion range. The semi-major (a) and semi-minor (b) axes of each elliptical beam spot along with the 'effective' radius (i.e. the radius of a circle with the same area as the ellipse) are shown. The ellipse described by 'a' and 'b' is the one that contains 95% of the beam.

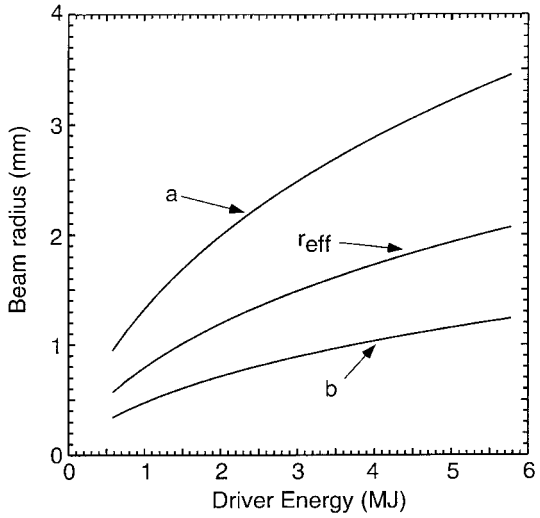

Figure 15. Beam spot sizes as a function of driver energy for the close coupled case to capsule ratio. The curves are for 250 eV drive and fixed ion range. The semi-major (a) and semi-minor (b) axes of each elliptical beam spot along with the 'effective' radius (i.e. the radius of a circle with the same area as the ellipse) are shown. The ellipse described by 'a' and 'b' is the one that contains 95% of the beam.

is absorbed by the capsule. By doing so, we reduce the amount of beam energy that the driver needs to deliver by almost a factor of two. This should have a significant impact on the cost of the driver. Since the driver is the single largest item in a power plant, this should also have an significant impact on the cost of electricity.

While the close coupled target reduces the amount of beam energy the driver has to deliver, it also requires a smaller beam focal spot than the conventional distributed radiator targets. This puts renewed emphasis on achieving high beam quality in the accelerator by controlling emittance growth, instability growth, etc. This target shows the benefit that can be achieved if the accelerator can deliver a small spot. In the final stage, the integrated system of accelerator, final focus, chamber transport and target will have to be optimized.

In addition to a smaller driver for a power plant, the close coupled target opens up the possibility of a high gain ETF from a 1.5–2 MJ driver. The ETF, which would be a step along the path to a fusion power plant, would be able to test all the physics and technology needed for a power plant. Our calculations predict that a smaller version of the close coupled target could achieve a gain of 94 from 1.75 MJ of beam energy. This target stressed the beam quality required from the accelerator even further since it requires a smaller spot and a shorter pulse duration.

Finally, we have presented gain curves for both the conventional distributed radiator and close coupled distributed radiator targets. These curves are useful for optimizing the entire system of accelerator, final focus, target and reactor chamber.

Acknowledgements

This work was performed under the auspices of the USDOE by Lawrence Livermore National Laboratory under Contract No. W-7405-ENG-48.

References

[1] Bodner, S.E., et al., Phys. Plasmas **5** (1998) 1901.
[2] Gardner, J.H., et al., Phys. Plasmas **5** (1998) 1935.
[3] Moir, R.W., et al., Fusion Technol. **25** (1994) 5.
[4] Zimmerman, G.B., Kruer, W.L., Comments Plasma Phys. Control. Fusion **2** (1975) 51.
[5] Tabak, M., Callahan-Miller, D., Ho, D.D.-M., Zimmerman, G.B., Nucl. Fusion **38** (1998) 509.
[6] Tabak, M., Callahan-Miller, D.A., Phys. Plasmas **5** (1998) 1896.
[7] Callahan-Miller, D.A., Tabak, M., Nucl. Fusion **39** (1999) 883.
[8] Haan, S.W., Phys. Plasmas **2** (1995) 2480.
[9] Krauser, W.J., et al., Phys. Plasmas **3** (1996) 2084.
[10] Suter, L.J., Amendt, P.A., Jones, O., Pollaine, S., Tabak, M., Bull. Am. Phys. Soc. **43** (1998) 1736.
[11] Lindl, J., Phys. Plasmas **2** (1995) 3933.
[12] Dittrich, T.R., Haan, S.W., Pollaine, S., Burnham, A.K., Strobel, G.L., Fusion Technol. **31** (1997) 402.
[13] Meier, W.R., "Systems modeling and analysis of heavy ion drivers for inertial fusion energy", paper presented at 13th Am. Nucl. Soc. Top. Mtg on the Technology of Fusion Energy, Nashville, TN, 1998.
[14] Campbell, E.M., Lawrence Livermore Natl Lab., CA, personal communication, 1998.
[15] Meier, W.R., Hogan, W.J., in Fusion Engineering (Proc. 15th Symp. Hyannis, 1993), IEEE, Piscataway, NJ (1994) 1001.
[16] Ho, D.D.-M., Lindl, J.D., Tabak, M., Nucl. Fusion **34** (1994) 1081.

(Manuscript received 22 March 1999
Final manuscript accepted 6 September 1999)

E-mail address of D.A. Callahan-Miller:
debbie@icf.llnl.gov

Subject classification: L0, Id; L0, It